6-25-2010

Characterization of aerosol associated with enhanced small particle number concentrations in a suburban forested environment

L. D. Ziemba
University of New Hampshire, Durham

Robert J. Griffin
University of New Hampshire, Durham

L. D. Cottrell
University of New Hampshire, Durham

Pieter J. Beckman
University of New Hampshire, Durham

Q. Zhang
State University of New York at Albany

Comments
This is an article published by AGU in Journal of Geophysical Research: Atmospheres in 2010, available online:
https://dx.doi.org/10.1029/2009JD012614

JOURNAL OF GEOPHYSICAL RESEARCH, VOL. 115, D12206, doi:10.1029/2009JD012614, 2010

Characterization of aerosol associated with enhanced small particle number concentrations in a suburban forested environment

L. D. Ziemba,[1,2] R. J. Griffin,[1,3] L. D. Cottrell,[1,4] P. J. Beckman,[1] Q. Zhang,[5,6] R. K. Varner,[1,7] B. C. Sive,[1] H. Mao,[1] and R. W. Talbot[1]

Received 8 June 2009; revised 8 February 2010; accepted 4 March 2010; published 25 June 2010.

[1] Two elevated particle number/mass growth events associated with Aitken-mode particles were observed during a sampling campaign (13–29 September 2004) at the Duke University Free-Air CO_2 Enrichment facility, a forested field site located in suburban central North Carolina. Aerosol growth rates between 1.2 and 4.9 nm hr^{-1} were observed, resulting in net increases in geometric mean diameter of 21 and 37 nm during events. Growth was dominated by addition of oxidized organic compounds. Campaign-average aerosol mass concentrations measured by an Aerodyne quadrupole aerosol mass spectrometer (Q-AMS) were 1.9 ± 1.6 (σ), 1.6 ± 1.9, 0.1 ± 0.1, and 0.4 ± 0.4 $\mu g\ m^{-3}$ for organic mass (OM), sulfate, nitrate, and ammonium, respectively. These values represent 47%, 40%, 3%, and 10%, respectively, of the measured submicron aerosol mass. Based on Q-AMS spectra, OM was apportioned to hydrocarbon-like organic aerosol (HOA, likely representing primary organic aerosol) and two types of oxidized organic aerosol (OOA-1 and OOA-2), which constituted on average 6%, 58%, and 36%, respectively, of the apportioned OM. OOA-1 probably represents aged, regional secondary organic aerosol (SOA), while OOA-2 likely reflects less aged SOA. Organic aerosol characteristics associated with the events are compared to the campaign averages. Particularly in one event, the contribution of OOA-2 to overall OM levels was enhanced, indicating the likelihood of less aged SOA formation. Statistical analyses investigate the relationships between HOA, OOA-1, OOA-2, other aerosol components, gas-phase species, and meteorological data during the campaign and individual events. No single variable clearly controls the occurrence of a particle growth event.

Citation: Ziemba, L. D., R. J. Griffin, L. D. Cottrell, P. J. Beckman, Q. Zhang, R. K. Varner, B. C. Sive, H. Mao, and R. W. Talbot (2010), Characterization of aerosol associated with enhanced small particle number concentrations in a suburban forested environment, *J. Geophys. Res.*, *115*, D12206, doi:10.1029/2009JD012614.

1. Introduction

[2] Aerosol particles are critically important in the atmosphere due to their ability to act as the nuclei around which liquid and ice clouds form and because of their ability to scatter or absorb radiation, thereby, affecting the radiative balance at the surface of the Earth [*Charlson et al.*, 1992]. The capacity of these particles to cause light extinction also leads to visibility degradation in affected areas [e.g., *Schichtel et al.*, 2001]. In addition, such aerosol particles provide surface area upon which heterogeneous reactions of atmospheric relevance occur [e.g., *Cwiertny et al.*, 2008] and have been associated with increased rates of morbidity and mortality among exposed populations [e.g., *Schwartz et al.*, 1996]. Lastly, deposition to the Earth's surface of particles represents a pathway for interphase transport of material within the Earth system [e.g., *Jordan and Talbot*, 2000]. It is thus important to increase understanding of the formation, chemistry, and processing of the associated particles.

[3] In recent work, it has been demonstrated that new particle formation occurs frequently throughout the entire troposphere, including the mixed layer closest to the Earth's surface [*Kulmala et al.*, 2004]. These particles grow by coagulation and condensation to sizes large enough to par-

[1]Climate Change Research Center, University of New Hampshire, Durham, New Hampshire, USA.
[2]Now at NASA Langley Research Center, Hampton, Virginia, USA.
[3]Now at Department of Civil and Environmental Engineering, Rice University, Houston, Texas, USA.
[4]Now at Environ, Groton, Massachusetts, USA.
[5]Atmospheric Sciences Research Center, State University of New York at Albany, Albany, New York, USA.
[6]Department of Environmental Toxicology, University of California, Davis, California, USA.
[7]Complex Systems Research Center, University of New Hampshire, Durham, New Hampshire, USA.

0148-0227/10/2009JD012614

ticipate in processes affecting human health and climate as described above. Consequently, it is important to understand both the conditions that favor small particle formation and the conditions that favor particle growth in a variety of environments. Of particular interest is the role played by organic components because inorganic species, such as sulfate, often are not able to account completely for particle formation and growth based on mass balance calculations [*Smith et al.*, 2008]. Using an Aerodyne quadrupole aerosol mass spectrometer (Q-AMS), organic compounds were identified as the major constituent of sub-100 nm diameter aerosol following new particle formation events at a forested site in southern Finland [*Allan et al.*, 2006]. In a more polluted atmosphere near Pittsburgh, PA, ammonium and sulfate contributed the majority of condensable mass during the early stages of growth events; however, photochemically produced secondary organic aerosol (SOA) contributed significantly to growth during later stages of these events [*Zhang et al.*, 2004, 2005]. In contrast, *Hock et al*. [2008] observed a growth event in rural southern Germany with significant mass contribution from aerosol nitrate.

[4] Volatile organic compounds (VOCs) that are biogenic in nature are emitted to the atmosphere on a global scale at a rate that is an order of magnitude larger than those of an anthropogenic nature [*Guenther et al.*, 1995]. Many of these biogenic VOCs (BVOCs) have been shown to be efficient precursors of SOA; SOA forms from the partitioning to the particulate phase (via condensation, heterogeneous uptake, and other mechanisms) of the oxidation products of the primary VOCs [*Seinfeld and Pankow*, 2003]. Despite numerous studies investigating this phenomenon, many uncertainties remain regarding new particle formation, SOA yields, and product identification [*Hallquist et al.*, 2009]. Because populated locations do not have a single source of aerosol precursors, continued studies aimed at understanding the role of both BVOCs and anthropogenic VOCs in particle growth are warranted; this topic is the focal point of the current manuscript.

2. Methods

[5] An investigation of VOC-SOA chemistry was conducted at the Duke University Forest-Atmosphere Carbon Transfer and Storage facility, specifically within the Free-Air CO_2 Enrichment (FACE) section, from 13–29 September 2004. The FACE site is located at 35°58′N and 79°05′W and lies approximately 160 m above sea level. The area contains three typical types of vegetation: a field of herbaceous vegetation that is mowed annually, a pine plantation planted in 1983 but that currently contains more than 40 woody species, and an oak-hickory forest. The most common species present, and therefore likely to influence BVOC-SOA chemistry, are loblolly pine, shortleaf pine, and Virginia pine. Based on loblolly pine emissions, the sesquiterpene β-caryophyllene and monoterpenes α-pinene and β-pinene are expected to be the primary BVOC affecting SOA formation at the FACE site [*Helmig et al.*, 2006]. The site is located approximately 2 km west of an interstate highway and 8 and 16 km from the moderately populated cities of Chapel Hill, NC, and Durham, NC, respectively. As a result, local anthropogenic emissions also are expected to influence SOA formation.

2.1. Measurements

[6] Aerosol measurements were collected at the base of towers erected inside two of the FACE site tree rings, one with ambient CO_2 and the other with CO_2 enriched (during the daytime) to approximately twice the ambient level. Bulk sample was drawn from a tower at a constant laminar flow rate of 10 L min^{-1} through a 1.27-cm outer diameter length of copper tubing with a University Research Glass (Chapel Hill, NC) 2.5 μm cyclone on the inlet. Aerosol instruments subsampled from this flow. Because aerosol measurements were only possible at one location at a time, no contemporaneous comparison between rings is possible, and the data are presented as a single time series with a break in the middle when instrumentation was moved from one ring (ambient) to the other (enriched). Therefore, this study is unable to investigate how changes in BVOC emission as a result of enriched CO_2 [*Naik et al.*, 2004] affect SOA formation. Efforts to sample at two different heights (16 and 20 m above ground) and investigate fluxes using the aerosol equipment showed no statistically significant differences in concentration; therefore, the data were composited into a single time series in this manner as well.

[7] Aerosols were characterized by a Q-AMS [*Jayne et al.*, 2000]. The Q-AMS provided size-resolved mass composition data of nonrefractory (based on a vaporization temperature of 550°C) aerosol species averaged over 10 min sampling periods. As in our previous work [*Cottrell et al.*, 2008], it is assumed that the presence of the cyclone did not affect the mass concentrations measured by the Q-AMS, as particles larger than a micrometer mostly are not transmitted through the aerodynamic focusing lens on the instrument inlet. The Q-AMS was subsampled isokinetically from the inlet line at approximately 140 mL min^{-1}.

[8] Principles of operation and analyses associated with the Q-AMS have been described in great detail elsewhere [*Jayne et al.*, 2000; *Jimenez et al.*, 2003; *Canagaratna et al.*, 2007]. Therefore, only a brief overview is given here. Ambient-pressure sample containing aerosol particles enters the instrument through a 130 μm critical orifice, after which particles are collimated using the aerodynamic focusing lens mentioned above [*Liu et al.*, 1995a, 1995b]. Because of the transmission efficiency of this lens, the Q-AMS measures particles with vacuum aerodynamic diameters (D_{va}) between 40 nm and 1 μm; this measurement is typically referred to as submicron [*Liu et al.*, 1995a, 1995b; *Jayne et al.*, 2000; *Allan et al.*, 2003], although the range of 100% transmission of particles is 60 to 600 nm. No correction was applied to account for sub-100% transmission of particles with diameters smaller than 60 and greater than 600 nm. This assumes that the bulk of the submicron particle mass resides between 60 and 600 nm [*Allan et al.*, 2003]. The resulting particle beam traverses a vacuum chamber of known dimension; during operation of the Q-AMS in particle-time-of-flight (pTOF) mode, measuring the travel time across this distance allows for calculation of chemical composition (for a subset of mass-to-charge (m/z) ratios) as a function of D_{va}. Size calibrations were performed using National Institute of Standards-traceable polystyrene latex spheres before and after the campaign.

[9] At the end of the vacuum chamber, particles are collected and vaporized on a resistively heated surface;

vaporized material is ionized under a 70 eV electron impact ionization source. When the Q-AMS was operating in mass spectrum mode (alternating with the pTOF mode), these ions were filtered by their m/z ratio in a Balzers (Balzers, Lichtenstein) QMA 410 quadrupole mass spectrometer and detected with a secondary electron multiplier. The Q-AMS scanned the m/z spectrum from 1 to 300 atomic mass units (amu) at 1 amu ms^{-1}. Mass/ionization efficiency calibrations of the Q-AMS were performed on-site every 2 to 3 days during the campaign using monodisperse ammonium nitrate aerosol, as described previously [*Cottrell et al.*, 2008].

[10] The algorithms described in the study of *Jimenez et al.* [2003] and *Allan et al.* [2003, 2004] were used to process all data collected during this study. The particle collection efficiency for the Q-AMS in this study appeared to be unity based on a regression (slope = 0.97, R^2 = 0.92) between Q-AMS sulfate (x variable) and sulfate aerosol determined by ion chromatographic analysis of the submicron stages of a colocated impactor (y variable); thus, no correction was made to account for particle bounce effects during heating/vaporization. For this study (10 min averages), the lower detection limits (LDLs) of the Q-AMS were 0.02 $\mu g\ m^{-3}$, 0.11 $\mu g\ m^{-3}$, 0.01 $\mu g\ m^{-3}$, and 0.14 $\mu g\ m^{-3}$ for sulfate, ammonium, nitrate, and organic material, respectively. Based on intercomparison of several Q-AMS instruments with other colocated instruments, an uncertainty of ±25% likely is applicable to the Q-AMS data presented here [*Canagaratna et al.*, 2007].

[11] Additional spectral analyses were performed in order to provide insight into the nature of the organic aerosol measured with the Q-AMS during the campaign. A deconvolution technique was also performed to apportion Q-AMS measured organic aerosol to hydrocarbon-like organic aerosol (HOA, thought to represent primary organic aerosol from combustion (motor vehicles, biomass burning), industry, etc.) and two types of oxygenated organic aerosol (OOA, thought to represent SOA in various states of aging) [*Zhang et al.*, 2007]. In addition, a Δ analysis [*McLafferty and Turecek*, 1993; *Drewnick et al.*, 2004] was conducted in which the predominance of different m/z signals is used to indicate the probable lability, size, and functionality of detected fragments. Intensities from positive Δ values indicate more oxygenated species, while negative Δ values result from cyclic, unsaturated, and aromatic compounds.

[12] Additional aerosol measurements performed during this campaign included those of black carbon (BC, for evidence of combustion) using a Magee Scientific (Berkeley, Calif) aethalometer and 24 h resolution 8 stage (plus backup filter) impactor samples. Impactor samples were extracted and analyzed off-line using an ion chromatograph for ammonium, potassium, magnesium, chloride, nitrate, and sulfate. Ion chromatographic extraction and analysis methods are described by *DeBell et al.* [2004]. These data were used for verification of the Q-AMS collection efficiency (described above) and to identify potential periods of atypical contributions from biomass burning (potassium), sea salt (chloride), or soil dust (magnesium).

[13] For quantification of mixing ratios of VOCs, hourly samples were collected from two inlet heights on the tower (also 16 and 20 m) using evacuated, polished stainless steel canisters. The gas collected in these canisters was analyzed off-line using the gas chromatographic system with several columns and detectors described by *Sive et al.* [2005] and *White et al.* [2010], allowing for accurate quantification of over 100 different VOC compounds. Specifically, α-pinene and isoprene are used as indicators of BVOC precursors to SOA [*Hoffmann et al.*, 1997; *Kroll et al.*, 2006], toluene is used as an indicator of a mixed biogenic-anthropogenic [*White et al.*, 2009] primary aromatic precursor to SOA [*Odum et al.*, 1997], and isopropyl nitrate is used as an additional indicator of secondary processing of anthropogenic emissions [*deGouw et al.*, 2005].

[14] Additional gases were measured from the base of the towers. Ozone (O_3) was measured using a miniature O_3 detector that operated on the principle of light absorption [*Mao et al.*, 2006]; like isopropyl nitrate, O_3 is used as a tracer of photochemical activity but without insight into relative contributions of biogenic and anthropogenic precursors. When enhanced, nitric oxide (NO) measured using a chemiluminescent technique (Thermo Environmental Instruments (Woburn, Mass) Model 42C-TL) also provides an indication of local combustion activities.

[15] Meteorological parameters collected routinely at the FACE sites are used to characterize overall atmospheric conditions at the times of data collection. These include temperature, wind speed, wind direction, and the flux of photosynthetically active radiation (PAR). PAR is used in this study as a surrogate for total solar radiation and strength of photochemical activity.

2.2. Event Definition

[16] Events characterized by enhanced contribution of small particles to aerosol mass were identified in the following manner. Without a measurement of aerosol particle number concentration, such values ($N(D_{va})$, cm^{-3}) were estimated for each D_{va} from the Q-AMS data, assuming the diameter of a spherical particle is equal to D_{va} divided by the aerosol density (ρ), by

$$N(D_{va}) = 10^9 \frac{6M_{D_{va}}\rho^2}{D_{va}^3\pi}, \quad (1)$$

where M_{Dva} is the total Q-AMS mass concentration ($\mu g\ m^{-3}$) of aerosol (consisting of sulfate, ammonium, nitrate, and organic material) associated with size D_{va} (nm). Note that $N(D_{va})$ is a lower limit particle number concentration for particles in the 40 to 1000 nm D_{va} range due to decreased inlet transmission outside of the 60 to 600 nm range. Values for ρ were estimated based on a weighted average calculation using mass concentrations measured by the Q-AMS [*Zhang et al.*, 2005] by

$$\rho = \rho_{org}\left(\frac{M_{org}}{M_{org}+M_{sulf}+M_{nitr}+M_{amm}}\right) + \rho_{inorg}\left(\frac{M_{sulf}+M_{nitr}+M_{amm}}{M_{org}+M_{sulf}+M_{nitr}+M_{amm}}\right), \quad (2)$$

where ρ_{org} is the density of pure organic aerosol (assumed to be $1.2 \times 10^{-15}\ \mu g\ nm^{-3}$), ρ_{inorg} is the density of pure inorganic aerosol (assumed to be $1.77 \times 10^{-15}\ \mu g\ nm^{-3}$), and M_{org}, M_{sulf}, M_{nitr}, and M_{amm} are mass concentrations of organic compounds, sulfate, nitrate, and ammonium, respectively. An average ρ of $1.47 \times 10^{-15}\ \mu g\ nm^{-3}$ (1.47 g cm^{-3}) was

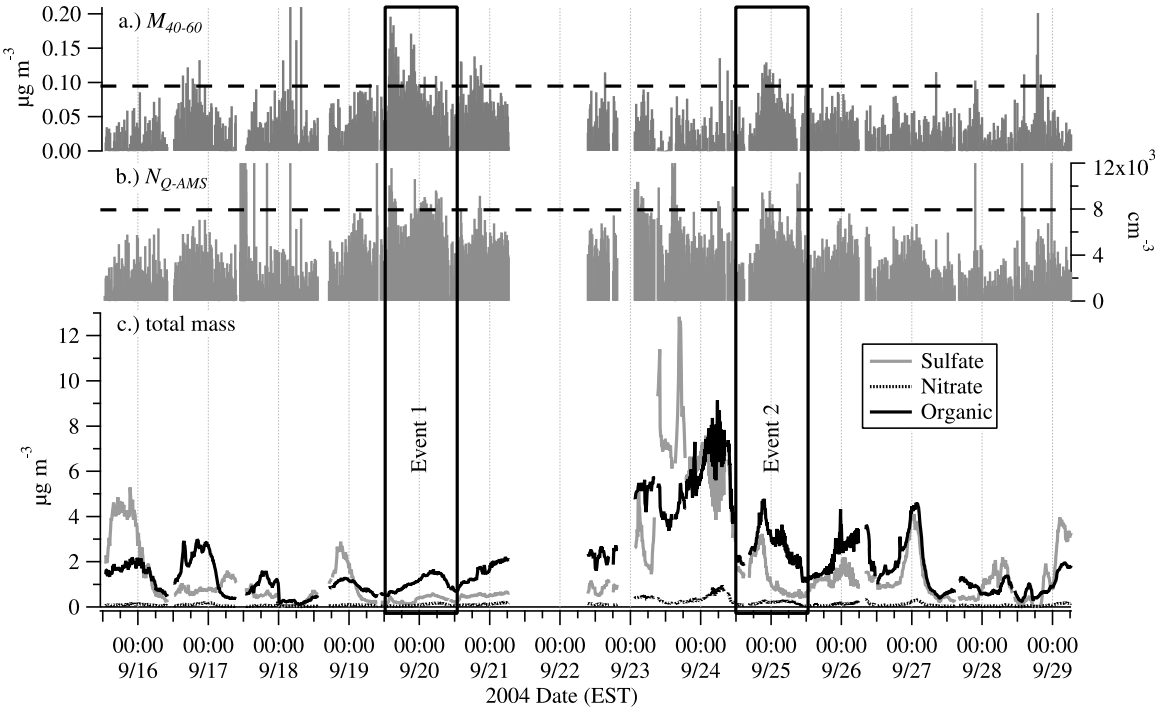

Figure 1. Time series of (a) $M_{40–60}$, (b) $N_{Q\text{-}AMS}$, and (c) Q-AMS measured aerosol mass concentrations over the course of the campaign. Events as described in the text are highlighted by boxes around the 24 h event day. Dotted lines represent threshold 95th percentile values of (a) 0.0947 μg m^{-3} and (b) 7930 cm^{-3}.

calculated for the campaign. Spherical aerosol particles are assumed, and this analysis ignores the contribution of liquid water content. From $N(D_{va})$, a total number concentration ($N_{Q\text{-}AMS}$) at each time was calculated by integrating over the Q-AMS detectable particle size space. An event was selected based on $N_{Q\text{-}AMS}$ and the mass concentration of the smallest detectable aerosol ($M_{40–60}$) using the Q-AMS (D_{va} larger than 40 nm and smaller than 60 nm). An event was defined as having concentrations that exceeded the campaign-average 95th percentile for both $M_{40–60}$ and $N_{Q\text{-}AMS}$ for a duration of more than 2 hours. The event day was defined as the 24 h (1200 to 1200 local time) during which the event occurred. $N_{Q\text{-}AMS}$, $M_{40–60}$, total aerosol mass concentrations, and the two selected events (henceforth referred to as E1 and E2, respectively) are shown in Figure 1.

[17] Particle growth is observed as a linear increase in the geometric mean diameter (GMD) of a log normally distributed aerosol population for particles with diameter less than approximately 60 nm, typically using a number-based size distribution measured by differential mobility analysis, as in the study of *Held et al.* [2004]. Here number-based aerosol size distributions are calculated using equation (1). The $N(D_{va})$ values during events were estimated from 1 h averaged Q-AMS data for organics, sulfate, and nitrate separately, resulting in a number size distribution for each chemical component. This distribution was then fit with a log normal curve. GMD was calculated as a function of chemical component according to *Mäkelä et al*. [2000]. The particle growth rate (GR) was determined for each component during each event by linear regression analysis, although linear behavior is not expected strictly for particle diameters greater than 60 nm.

2.3. Backward Trajectory Analysis

[18] In order to consider bulk air mass motion affecting the Duke FACE site during each of the particle number events, backward trajectories were calculated for the event days. The Hybrid Single-Particle Lagrangian Integrated Trajectory (HYSPLIT) model [*Draxler and Rolph*, 2003] was used to calculate 72 h backward trajectories originating at 1000 m above ground level directly over the FACE site; this height was used for consistency for all simulations given that data for boundary layer height were unavailable. Choice of this height also avoided air masses reaching the surface prematurely. For each event day, backward trajectories were calculated for air masses arriving at the site at 1200, 1600, 2000, 0000, 0400, and 0800 local (EDT) time. HYSPLIT was run using the archived 40 km Eta Data Assimilation System grid for meteorological input and assuming isobaric vertical motion.

3. Results

3.1. Campaign Overview

[19] An overview of Q-AMS measurements during the campaign is provided in Figure 1, which shows the time series of the major measured nonrefractory components of the submicron aerosol. As shown in Figure 1, aerosol mass loadings were highly variable. Mass concentrations over the entire campaign averaged 1.9 ± 1.6 (one standard deviation; median of 1.5, range of below LDL to 8.2), 1.6 ± 1.9

Table 1. Statistics of Measured Variables Over the Campaign and During Each Event Identified in the Text

	Campaign[a]	E1	E2
Date[b]	13–29 Sep	19–20 Sep	24–25 Sep
OM (μg m^{-3})	1.9 ± 1.6	1.0 ± 0.3	2.2 ± 0.7
HOA (μg m^{-3})	0.12 ± 0.15	0.06 ± 0.05	0.22 ± 0.16
OOA-1 (μg m^{-3})	1.2 ± 1.1	0.54 ± 0.15	1.5 ± 0.5
OOA-2 (μg m^{-3})	0.59 ± 0.49	0.45 ± 0.17	0.81 ± 0.35
HOA/sum[c]	0.06 ± 0.05	0.05 ± 0.03	0.08 ± 0.04
OOA-1/sum	0.58 ± 0.16	0.52 ± 0.06	0.60 ± 0.12
OOA-2/sum	0.36 ± 0.16	0.42 ± 0.05	0.32 ± 0.09
Sulfate (μg m^{-3})	1.6 ± 1.9	0.3 ± 0.1	1.0 ± 0.7
Ammonium (μg m^{-3})	0.4 ± 0.4	0.1 ± 0.0	0.3 ± 0.2
Nitrate (μg m^{-3})	0.1 ± 0.1	0.1 ± 0.0	0.1 ± 0.1
Neutralization[d]	1.6 (0.94)	1.2 (0.92)	1.5 (0.96)
Black carbon (ng m^{-3})	372.0 ± 289.3	162.4 ± 80.8	NA
Ozone (ppbv)	27.9 ± 14.9	31.0 ± 4.8	NA
Nitric oxide (pptv)	236.8 ± 536.8	163.5 ± 256.1	NA
Isoprene (pptv)	427.0 ± 561.9	190.1 ± 159.1	440.3 ± 386.8
α-Pinene (pptv)	456.6 ± 771.7	91.9 ± 46.0	250.6 ± 220.6
Toluene (pptv)	92.9 ± 62.0	53.1 ± 25.7	91.6 ± 37.4
Isopropyl nitrate (pptv)	3.8 ± 2.1	2.3 ± 0.3	5.0 ± 1.5
PAR[e] (μmol m^{-2} s^{-1})	836.8 ± 502.4	1285.2 ± 284.5	NA
Wind speed (m s^{-1})	2.1 ± 0.9	2.4 ± 0.8	NA
Wind direction (degrees)[f]	133.8 ± 95.8	87.3 ± 67.5	NA
Temperature (Celsius)	18.7 ± 4.6	14.2 v 4.5	NA

[a]Values shown are averages ± one standard deviation.
[b]Events are defined as noon to noon, local time, with campaign dates being general because some equipment were on-line sooner or later than others.
[c]Sum reflects HOA + OOA-1 + OOA-2.
[d]Expressed as the slope of a regression between molar ammonium and sulfate concentrations (such that 2.0 implies complete neutralization by ammonium) with R^2 given in parentheses.
[e]PAR values between 0800 and 1600 local time included.
[f]Zero degree = due north.
NA, not available for significant fraction of event day.

(median of 0.8, range of 0.02 to 12.5), 0.1 ± 0.1 (median of 0.1, range of 0.01 to 0.9), and 0.4 ± 0.4 (median of 0.2, range of below LDL to 2.9) μg m^{-3} for organic material, sulfate, nitrate, and ammonium (not shown in Figure 1), respectively. These lead to an overall average composition of 47%, 40%, 3%, and 10% for the four species, respectively. The ratios of the average to the median (which indicate the influence of very large concentrations if the values are significantly larger than unity) are 1.3, 1.9, 1.5, and 1.7 for organic material, sulfate, nitrate, and ammonium, respectively, indicating organic material was least subject to variability, potentially due to sampling within a forest environment. In general, the aerosol measured during the campaign was not fully neutralized by ammonium, with a slope of 1.6 for a regression between molar ammonium (y variable) and sulfate (x variable) concentrations. Campaign average parameters are shown in Table 1.

[20] The overall average contributions of specific m/z values to the organic signal over the course of the campaign are presented in Figure 2a. Of particular note are the strong, nearly equal signals at m/z 43 and 44 and elevated peaks at m/z 27 and 29, which are the main spectral features observed for biogenic SOA generated from the oxidation of VOC emissions from live plants [*Kiendler-Scharr et al.*, 2009]. The signal at m/z 44 in ambient aerosol MS primarily results from CO_2^+, which is thought typically to represent highly oxidized OOA, while m/z 43 (primarily $C_3H_7^+$ and $C_2H_3O^+$) is influenced by organic material of both primary and secondary nature [*Zhang et al.*, 2005; 2007]. The signals at m/z 41 and 55 result from HOA and, to a lesser extent, less oxidized OOA, and those at m/z 27 and 29 are thought to result from less oxidized OOA as well [*Zhang et al.*, 2005; 2007].

[21] Again, mass spectra with an increased contribution from m/z 44 compared to m/z 43 are typically associated with more oxidized OA [*Zhang et al.*, 2005; 2007]. (See comparisons of mass spectra in *Kiendler-Scharr et al.* [2009].) Still, it is difficult to separate quantitatively the sources of OA given the variability in the relative contributions from m/z 43 and m/z 44 and that the observed mass spectra at Duke Forest are likely a mixture of both local and regional sources. Therefore, for this study, the term "local" refers to sources within Duke Forest that are mostly biogenic but also include several smaller roadways surrounding the site. Likewise, the term "regional" refers to the broader area experiencing mixed biogenic/anthropogenic influences and that includes forested, suburban, and urban sections.

[22] The spectra from this study were compared to those of *Cottrell et al.* [2008] for a semirural New England location and *Allan et al.* [2006] for a Finnish boreal forest. The average spectrum shown in Figure 2a (x variable) correlated with that of *Cottrell et al.* [2008] (not shown, y variable) with a slope and R^2 of 0.98, suggesting very similar spectra. The comparison indicates a slightly increased relative contribution of m/z 44 compared to m/z 43 in the work of *Cottrell et al*. [2008], indicating that the aerosol sampled in that study was more oxidized and maybe more aged. Similarly, the spectrum presented by *Allan et al.* [2006] indicates an even larger relative signal of m/z 43 (compared to spectra from *Cottrell et al.* [2008]), showing that enhanced m/z 43 signal (without a corresponding increase at m/z 55) can be used to indicate SOA that is potentially biogenic in nature.

[23] The results of a Δ analysis across the entire campaign are shown in Figures 2b and 2c. Figure 2b indicates the overall average intensity of specific Δ values ($\Delta = m/z - 14n + 1$ where n is the nominal number of carbons in the fragment, that is, 1 for m/z from 12 to 23, 2 for m/z from 24 to 35, etc. [*McLafferty and Turecek*, 1993]), and shows the predominance of Δ values 2, 0, and 3 (due nominally to m/z 43 and 29, 41 and 27, and 44). Compared to values in southern New Hampshire [*Cottrell et al.*, 2008], the intensities of Δ values 0 and 2 at Duke Forest are enhanced, and the intensity at Δ value 3 is decreased. These changes correspond to the relative changes in m/z 43 and 44 between the two studies.

[24] Figure 2c indicates the segregation of average Δ values by n. The average Δ value for fragments with carbon number between one and four is approximately 0.7 (compared to 0.8 for the study of *Cottrell et al*. [2008]). The values for fragments with carbon numbers five and six and fragments with carbon numbers between 7 and 15 are −1.5 and −1.0 in this study compared to the values of −1.4 and −0.9 from the study of *Cottrell et al*. [2008]. The greater contribution of smaller fragments again indicates the aerosols observed by *Cottrell et al.* [2008] were more oxidized. The Δ patterns for both studies are similar to those observed for chamber-derived SOA from oxidation of α-pinene [*Bahreini et al.*, 2005] and biogenic SOA produced in a

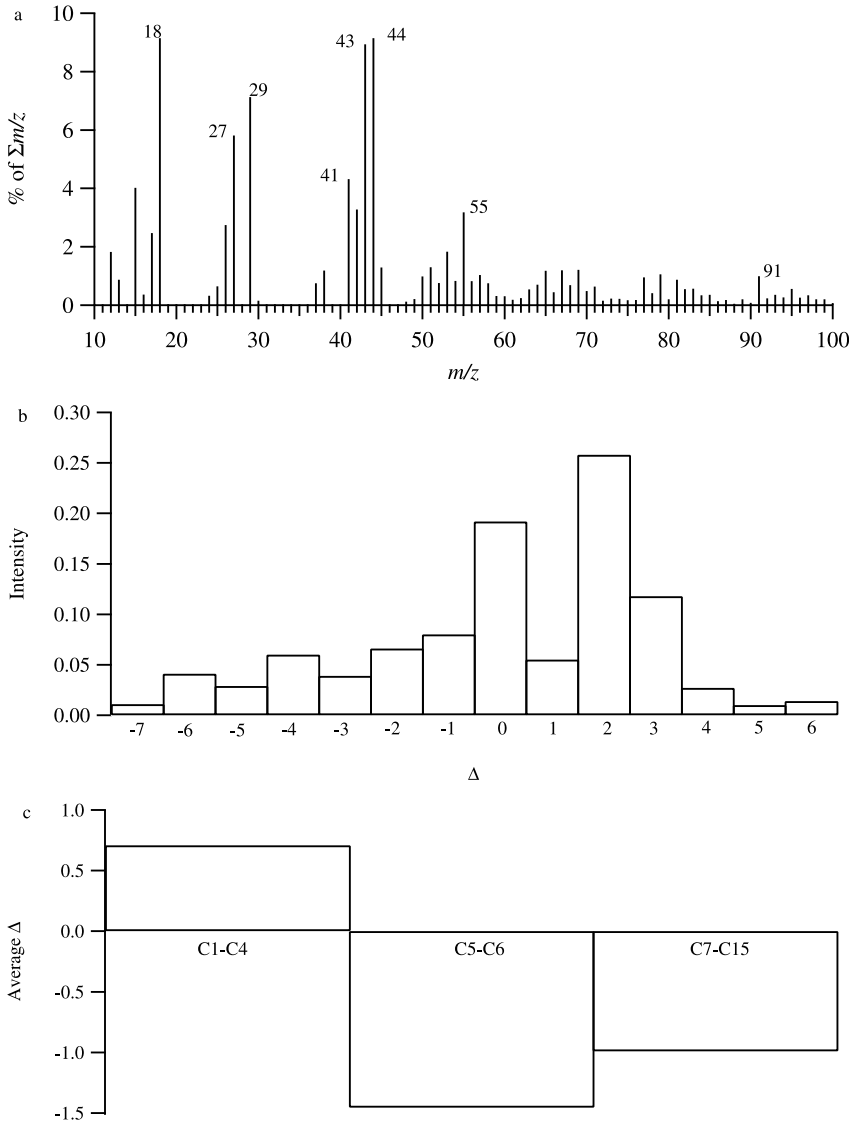

Figure 2. (a) Campaign average spectrum expressed as the contribution of specific m/z values to the total organic signal, (b) campaign-average intensities at specified Δ values, and (c) campaign-average Δ values segmented by carbon number.

chamber with live plant emissions [*Kiendler-Scharr et al.*, 2009], suggesting that BVOC played a role in the formation of SOA at the Duke Forest site but not discounting influence from regional and potentially anthropogenic sources.

[25] When the method of *Zhang et al.* [2007] was applied to the organic aerosol mass spectral matrix, three organic aerosol components were identified: one representing HOA (including contribution from biomass burning aerosol, henceforth, termed HOA/BBOA) and two representing OOA in separate states of oxidation/aging (OOA-1 and OOA-2) [*Zhang et al.*, 2007]. The spectra representing each of these components are shown in Figure 3. As would be expected based on previous studies, the HOA/BBOA spectrum shows elevated relative signal at m/z values 41 and 43 as well as 55, 57, and the last two m/z values plus 14 units, representing a CH_2 unit. The spectrum of OOA-1, again thought to indicate regional aged SOA, is dominated by signal at m/z 44. Lastly, the spectrum of OOA-2, thought to represent less oxidized SOA, potentially of a biogenic nature, shows enhanced relative signals at m/z 27, 29, and 43. To underscore the interpretation of this deconvolution, the time series of HOA/BBOA (y variable) was regressed against the contemporaneous time series of BC (x variable), with a resulting R^2 of 0.50, a value that indicates a probable shared source (both derived from combustion), though this relationship is not as strong as that observed in the study of *Cottrell et al.* [2008] during which a value of 0.76 was found. Similarly, a regression between sulfate aerosol and OOA-1 yields a R^2 value of 0.71 for this study, compared to 0.74 for the study of *Cottrell et al.* [2008], underscoring the probable regional nature of sulfate and OOA-1. These R^2 values are summarized in Table 2.

[26] The time series for the calculated concentrations of the organic aerosol components also are shown in Figure 3.

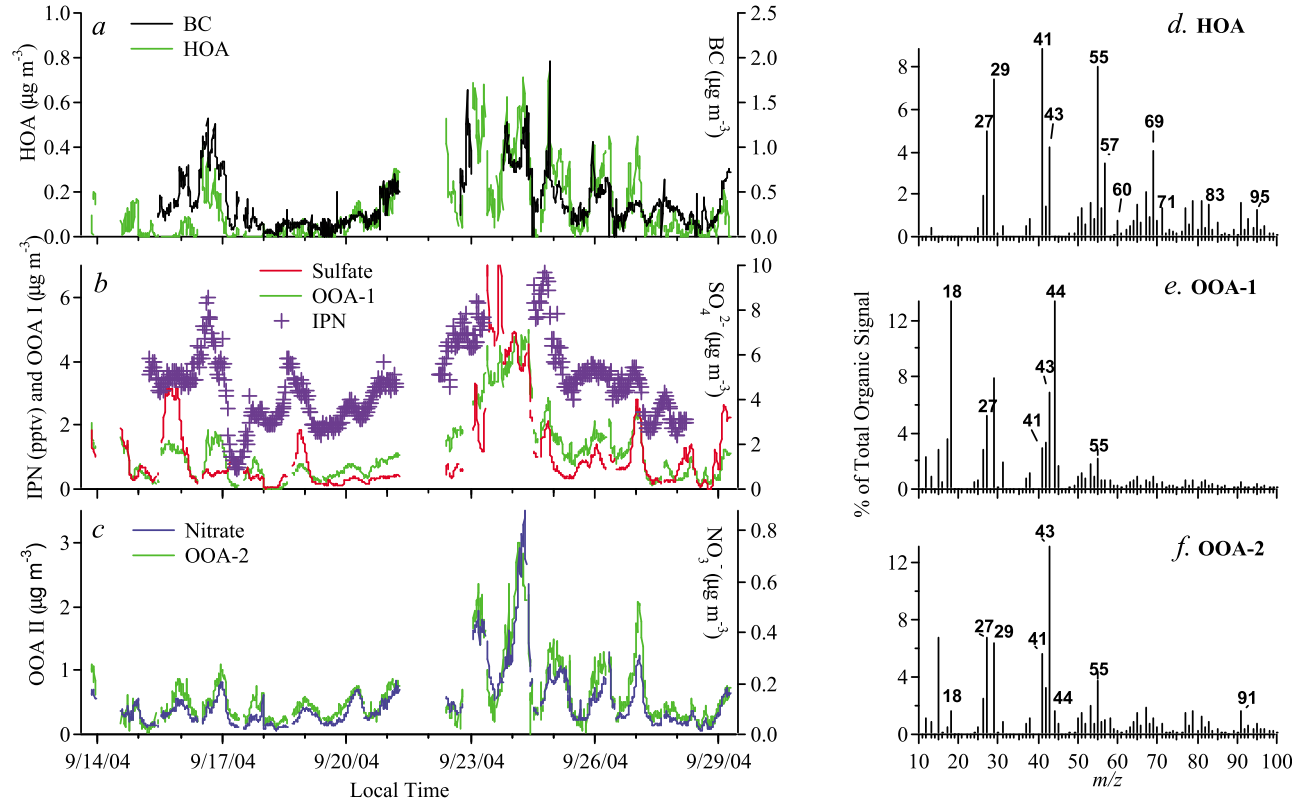

Figure 3. Time series of concentrations (μg m^{-3}) for derived components ((a) HOA/BBOA, (b) OOA-1, and (c) OOA-2) of organic aerosol measured by the Q-AMS. Other measured variables to which the components correlate are included. The corresponding derived average spectra (as in Figure 2a) are shown in Figures 3d, 3e, and 3f for HOA/BBOA, OOA-1, and OOA-2, respectively. Spectra were determined by the method of *Zhang et al.* [2007]. IPN represents isopropyl nitrate.

The average concentrations of HOA/BBOA, OOA-1, and OOA-2 are 0.12 ± 0.15 (median of 0.06, maximum 0.75), 1.2 ± 1.1 (median of 0.89, maximum 5.01), and 0.59 ± 0.49 (median of 0.44, maximum of 3.0) μg m^{-3}, respectively. The ratios of the average to the median are 1.9, 1.3, and 1.3, respectively, indicating that the components generally are affected to the same degree by large concentration events except for the surrogate for primary emissions. The average

Table 2. R^2 for Correlations Between Organic Aerosol Components and Other Measured/Derived Quantities Over the Course of the Campaign and for Each Event Identified in the Text[a]

Campaign	OOA-1	OOA-2	Sulfate	Nitrate	Ammonium	BC	NO	Toluene	Isoprene	α-Pinene	IPN[b]	O_3	Wind Speed	Wind Direction	Temperature	PAR[c]
HOA/BBOA	**0.50**	**0.67**	0.20	**0.63**	0.29	**0.50**	0.00	0.20	0.00	0.00	0.43	0.18	0.11	0.05	0.07	0.03
OOA-1		**0.81**	**0.71**	**0.66**	**0.79**	**0.51**	0.00	0.08	0.05	0.01	**0.84**	0.32	0.15	0.06	0.00	0.16
OOA-2			0.22	**0.82**	0.33	0.38	0.01	0.13	0.00	0.02	0.34	0.13	0.09	0.04	0.11	0.04

E1	OOA-1	OOA-2	Sulfate	Nitrate	Ammonium	BC	NO	Toluene	Isoprene	α-Pinene	IPN	O_3	Wind Speed	Wind Direction	Temperature	PAR
HOA/BBOA	0.28	**0.53**	0.27	**0.63**	0.34	0.43	0.03	**0.68**	0.36	0.02	0.27	0.11	0.08	0.03	0.42	0.45
OOA-1		**0.64**	**0.56**	**0.56**	**0.60**	0.24	0.08	0.25	**0.51**	0.01	**0.62**	**0.50**	0.39	0.00	**0.83**	**0.78**
OOA-2			**0.57**	**0.88**	0.21	0.37	0.00	**0.63**	**0.61**	0.03	**0.49**	0.33	0.21	0.00	**0.79**	**0.92**

E2	OOA-1	OOA-2	Sulfate	Nitrate	Ammonium	BC	NO	Toluene	Isoprene	α-Pinene	IPN	O_3	Wind Speed	Wind Direction	Temperature	PAR
HOA/BBOA	0.26	**0.54**	0.08	**0.58**	0.11	NA	NA	0.00	0.17	0.00	0.00	NA	NA	NA	NA	NA
OOA-1		0.08	**0.85**	0.03	**0.85**	NA	NA	0.03	0.32	0.01	**0.66**	NA	NA	NA	NA	NA
OOA-2			0.00	**0.69**	0.01	NA	NA	**0.70**	0.25	0.25	0.01	NA	NA	NA	NA	NA

[a]Values larger than 0.50 are shown in bold.
[b]Isopropyl nitrate.
[c]Values included only between 0800 and 1600 local time.
NA, not available for significant fraction of event day.

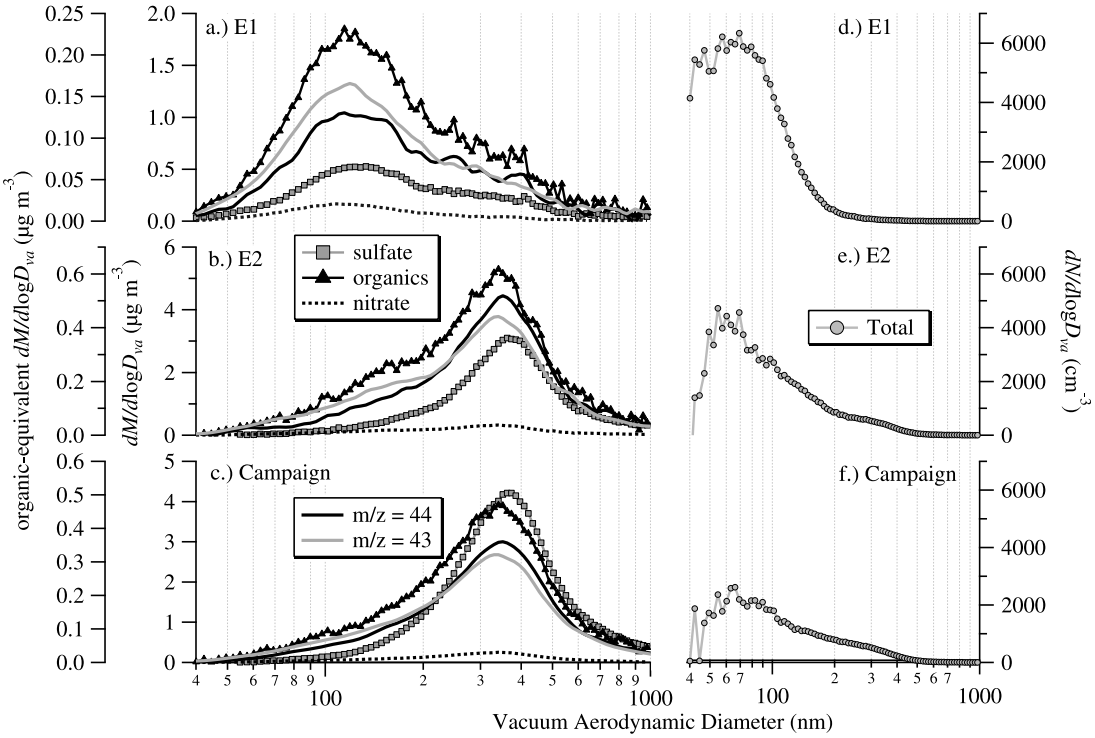

Figure 4. Average mass-based particle size distribution (dM/dlogD_{va}, μg m^{-3}) for (a) E1, (b) E2, and (c) the full campaign and total aerosol average number-based particle size distribution (dN/dlogD_{va}, cm^{-3}) for (d) E1, (e) E2, and (f) the full campaign. Note that dN/dlogD_{va} is likely underestimated at D_{va} less than 60 nm due to decreased sampling efficiency by the Q-AMS in this size range.

composition of the organic aerosol was 6% HOA/BBOA, 58% OOA-1, and 36% OOA-2.

[27] Figure 4 shows the chemically resolved mass-based particle size distribution (dM/dlogD_{va}, μg m^{-3}) and the total number-based particle size distribution (dN/dlogD_{va}, cm^{-3}) for the campaign and for each event. Organic-equivalent mass-size distributions of organic fragments at m/z = 44 and m/z = 43 are included in Figure 4 for E1, E2, and the full campaign. It is indicated in Figure 4c that inorganic aerosol constituents (nitrate and sulfate) exhibit similar behavior, with peaks in dM/dlogD_{va} between 300 and 400 nm in D_{va}. This size likely indicates transport of aged regional aerosol to the site [*Marquez et al.*, 2005]. Inorganic mass clearly is dominated by sulfate. In contrast, organic aerosol shows different behavior. The predominant peak is shifted to slightly smaller sizes relative to those of the inorganics; in addition, the distribution is significantly broader, with more pronounced contributions to mass from particles smaller than those at the peak of the distribution (Figures 4a–4c). dM/dlogD_{va} for m/z = 43 and m/z = 44 exhibited similar distributions although dM/dlogD_{va} for m/z = 43 was broader and greater than that of m/z = 44 at smaller D_{va} (<200 nm) for the full campaign (Figure 4c). This trend is especially exaggerated during E1 (Figure 4a) and to a lesser extent during E2 (Figure 4b).

[28] Calculated total number-based size distributions (dN/dlogD_{va}, cm^{-3}) for E1, E2, and the full campaign all have a maximum at 60–70 nm D_{va} (Figures 4d–4f). The magnitude of this peak is significantly increased during both events, by approximately a factor of 3 and 2 for E1 and E2, respectively. Additionally, the minor mode in dN/dlogD_{va} present during the full campaign and during E2 is negligible during E1.

[29] Data from the impactors can be used to investigate the influence of other aerosol sources on the submicron aerosol loading. Sulfate, as discussed above, was used to verify the collection efficiency of the Q-AMS. Here only the sub-1.1 μm stages of the impactor are composited and averaged. For the thirteen ~24 h impactor samples collected during the campaign, the concentrations of potassium (biomass burning), magnesium (soil/crustal), and chloride (fresh oceanic air) are used as indicators of other sources that may contribute to the submicron Q-AMS measurement of organic material. Over the course of the campaign, the blank-corrected concentrations of these three species averaged 12.3 ± 7.3 (median of 11.0, range of 2.5 to 28.7), 2.8 ± 2.1 (median of 2.6, range of 0.1 to 6.4), and 7.2 ± 6.6 (median of 3.8, range of 1.0 to 20.3) ng m^{-3}, respectively. In each case, the average to median ratio is less than two. The uncertainty associated with each measurement is 2.4, 0.6, and 3.1 ng m^{-3}, respectively. Because of these very small concentrations, influence of biomass burning, soil components, and sea salt on submicron organic aerosol are considered negligible.

[30] Data from the aethalometer can be used to indicate the typical influence of combustion sources at the site. Over the course of the entire campaign, the average BC concentration was 372 ± 289 (median of 285, range from below LDL of 4 to 1956) ng m^{-3}; on average, this indicates a BC concentration more than five times smaller than the Q-AMS observed organic aerosol and more than 10 times smaller than the total Q-AMS observed submicron aerosol. How-

ever, the presence of BC (with limited concentrations of potassium) and the average 7% contribution of HOA/BBOA to the overall organic aerosol mass loading indicate some variable (with a ratio of average to median of 1.3) influence of anthropogenic activities at the site. Similarly, enhanced mixing ratios of NO can be used to indicate local combustion sources, despite local soil and biogenic sources [*Ludwig et al.*, 2001; *Hari et al.*, 2003]. Over the campaign, the average value of NO mixing ratio was 0.2 ± 0.5 (median of 0.1) ppbv, and the corresponding range was from below the LDL of the instrument (approximately 75 pptv) to 4.7 ppbv, indicating a probable local combustion source. In general, NO mixing ratios were small, and it is likely that O_3 chemistry was NO_x-limited and that low-NO_x SOA yield parameters would be most appropriate [*Presto et al.*, 2005; *Song et al.*, 2005]. In addition, NO shows no relationship (Table 2) with any of the organic aerosol components.

[31] As stated previously, four (out of many) VOCs will be used to assess likely precursors to O_3 and SOA in the FACE site during the campaign and within the particle events, specifically. The campaign-average mixing ratios for toluene, isoprene, α-pinene, and isopropyl nitrate were 92.9 ± 62.0 (median of 76.7, range of 17.9 to 378.3), 427.0 ± 561.9 (median of 283.4, range of 2.6 to 6275.6), 456.6 ± 771.7 (median of 219.4, range of 19.2 to 7491.8), and 3.8 ± 2.1 (median of 3.4, range of 0.6 to 10.6) pptv, respectively. For these four compounds, the ratios of the average to the median were 1.2, 1.5, 2.1, and 1.1, respectively, indicating that BVOCs were subject to significantly greater variability, much of it diurnal in nature. Overall, the compound with the largest average and median mixing ratio was ethane, which would be expected due to its long lifetime. Considering reactivity (combining reaction rate constants and mixing ratios), isoprene and the monoterpene isomers (of the VOCs measured) had the greatest in situ impact on chemistry in the FACE site, as would be expected. In fact, α-pinene exhibited the greatest single mixing ratio observed over the course of the campaign.

[32] In an effort to understand any relationship between different types of organic aerosol and these VOCs, regressions were performed; these are summarized in Table 2. The primary VOCs are not correlated with any of the organic aerosol components (all R^2 less than or equal to 0.20). However, all three organic aerosol components show stronger correlation (R^2 greater than or equal to 0.34) with isopropyl nitrate, particularly OOA-1, with an R^2 of 0.84. The study of *deGouw et al.* [2005] indicated an R^2 of 0.69 for isopropyl nitrate with total organic aerosol thought to be mostly secondary; hence, isopropyl nitrate was used as an indicator of anthropogenic SOA. In this study, the relationships between isopropyl nitrate and OOA-1 and between OOA-1 and sulfate indicate the regional anthropogenic nature of the isopropyl nitrate. The strong relationship between HOA/BBOA and isopropyl nitrate indicates that NO_x from combustion sources is predominantly responsible for the isopropyl nitrate formation. The similar relationship between isopropyl nitrate and OOA-2 could indicate anthropogenic influence on less oxidized biogenic SOA formation, as hypothesized by *Tsigaridis and Kanakidou* [2007].

[33] Ozone mixing ratios also can be used as indicators of photochemistry, though without an indication of the relative influences of biogenic and anthropogenic emissions. Over the course of the Duke campaign, the O_3 mixing ratio ranged from 0.5 to 78.4 ppbv, with an average of 27.9 ± 14.9 and a median of 25.2. The ratio of the average to the median was 1.1. These values are not vastly different than those obtained when considering only the data from between 0800 and 1600 local time in order to account for the diurnal nature of O_3. The relationships between O_3 and the organic aerosol components are weak, with R^2 values all less than 0.33. For HOA/BBOA, this is intuitive as emissions are generally independent of photochemistry. The lack of a relationship with OOA-1 likely indicates that the air masses with enhanced OOA-1 are aged more than a day (because of the diurnal nature of O_3), which is consistent with the regional source of OOA-1. More interesting is the lack of a relationship between OOA-2 (representative of less oxidized and less aged SOA) and O_3. This is explained by any combination of the following: (1) only minimal gas phase photochemical activity is needed to form OOA-2 instantaneously at this site, (2) additional processing time (i.e., multiple generations of oxidation) is necessary to form products that are more likely to participate in gas-to-particle partitioning, (3) gas-to-particle conversion of VOC at the site may be most sensitive to changes in temperature (during E1 for example) and not precursor availability, and (4) OOA-2 also is aged more than one day but still is aged less than OOA-1. Although nitrogen dioxide (NO_2) is not included in this analysis due to a lack of measurements, it is assumed that its mixing ratios are small based on the relative mixing ratios of O_3 and NO. Therefore, it does not appear that OOA-2 would exhibit a strong relationship with O_x (O_3 + NO_2) as well, which is in contrast to measurements made by *Herndon et al.* [2008] in Mexico City.

[34] Relationships with meteorological parameters may also provide some insight into the nature/source of the three organic aerosol components; regression coefficients are also shown in Table 2. Wind speed (generally on the order of 1–2 m s^{-1}), wind direction (predominantly from the east/southeast), temperature (typically around 20°C), and PAR (maximum of 1878.7 μmol m^{-2} s^{-1}) show no relationship with any of the three organic aerosol components, indicating the regional and aged nature of air masses containing HOA/BBOA and OOA-1. It is hypothesized that PAR would show the strongest relationship with OOA-2, given that local SOA formation is often driven by local photochemical conditions. However, as with O_3, no strong relationship is shown between OOA-2 and PAR over the course of the campaign. When only daytime (0800–1600 local) PAR is considered (836.8 ± 502.4 mmol m^{-2} s^{-1}, median of 848.2, and range of 38.7 to 1878.7), the relationship between the organic aerosol components and PAR does not strengthen considerably, with R^2 values of 0.03, 0.16, and 0.04 for HOA/BBOA, OOA-1, and OOA-2, respectively. These poor relationships again indicate the regional/aged nature of HOA/BBOA and OOA-1 and suggest the potential importance of higher generation oxidation products to SOA formation, which may result in a lag time between maximum PAR and SOA. It is also possible that the correlation between PAR and OOA-2 could be affected by the coupling between PAR and temperature. OOA-2 is expected to evaporate under elevated temperatures due to its semivolatile nature [*Lanz et al.*, 2007; *Ulbrich et al.*, 2009]. Vertical daytime mixing also could complicate these relationships.

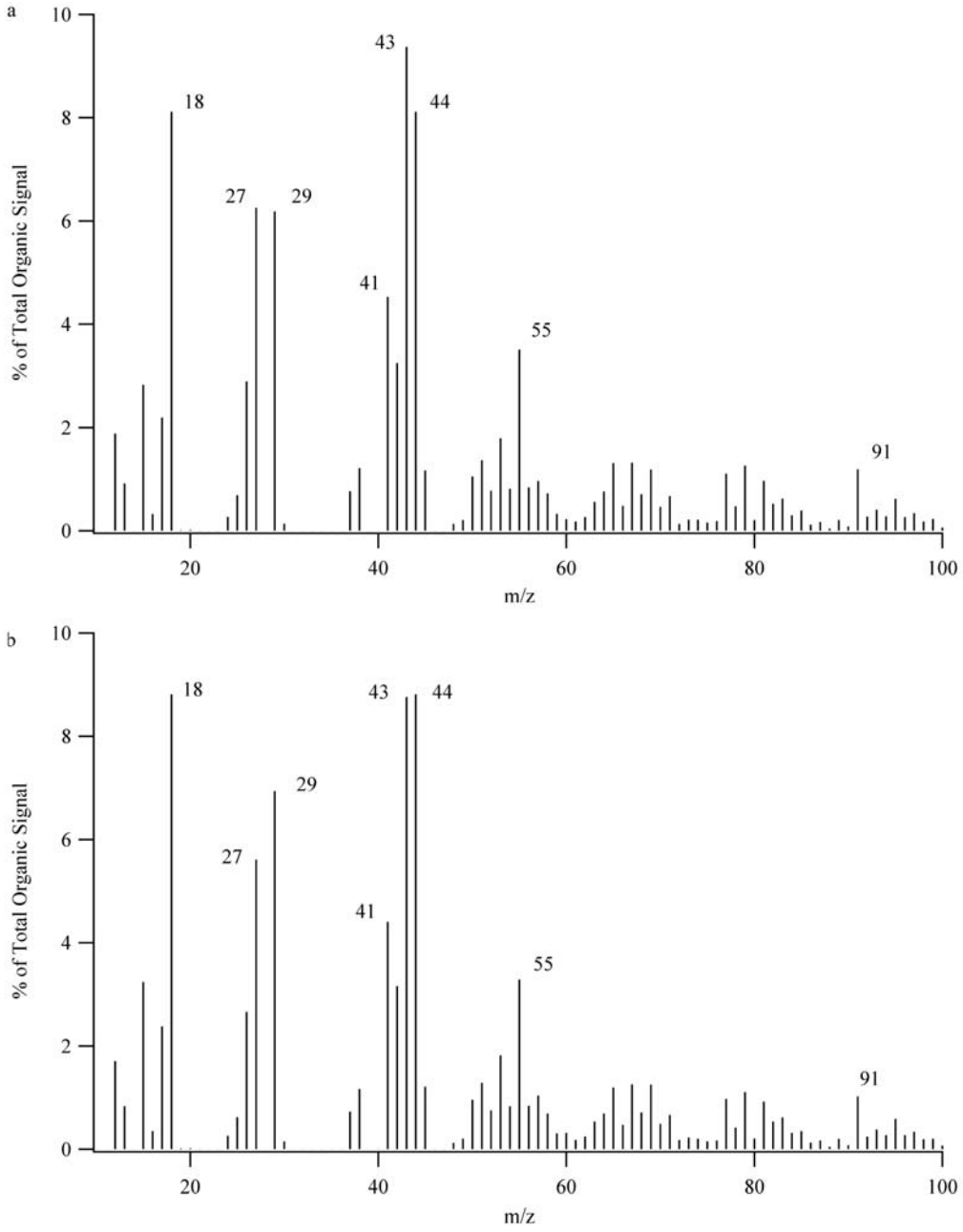

Figure 5. Average mass spectra as in Figure 2a for each of the events discussed in the text: (a) E1 and (b) E2.

3.2. Events

[35] Over the course of the campaign, two events were identified according to the criteria outlined previously. The corresponding event days were 19–20 September (again defined as 1200 to 1200 local) and 24–25 September, as shown in Table 1 and highlighted in Figure 1. The average mass concentrations of the aerosol species (both measured and calculated), mixing ratios of gaseous pollutants, and values for meteorological parameters are summarized in Table 1 for each event. Table 2 includes the R^2 values for regressions between parameters within a given event.

3.2.1. E1

[36] Compared to the average, E1 exhibited decreased total concentrations of OM, HOA/BBOA, OOA-1, OOA-2, sulfate, ammonium, nitrate, and BC in the observed aerosols. The increased fractional contribution of OOA-2 to the overall organic mass (OM) is confirmed by the spectrum indicated in Figure 5a that shows enhancement at m/z 43. In addition, the aerosol in E1 appears to be less neutralized with respect to ammonium. During E1, the mixing ratios of O_3 were comparable to the campaign average, but other gases (NO and VOCs) exhibited mixing ratios that were

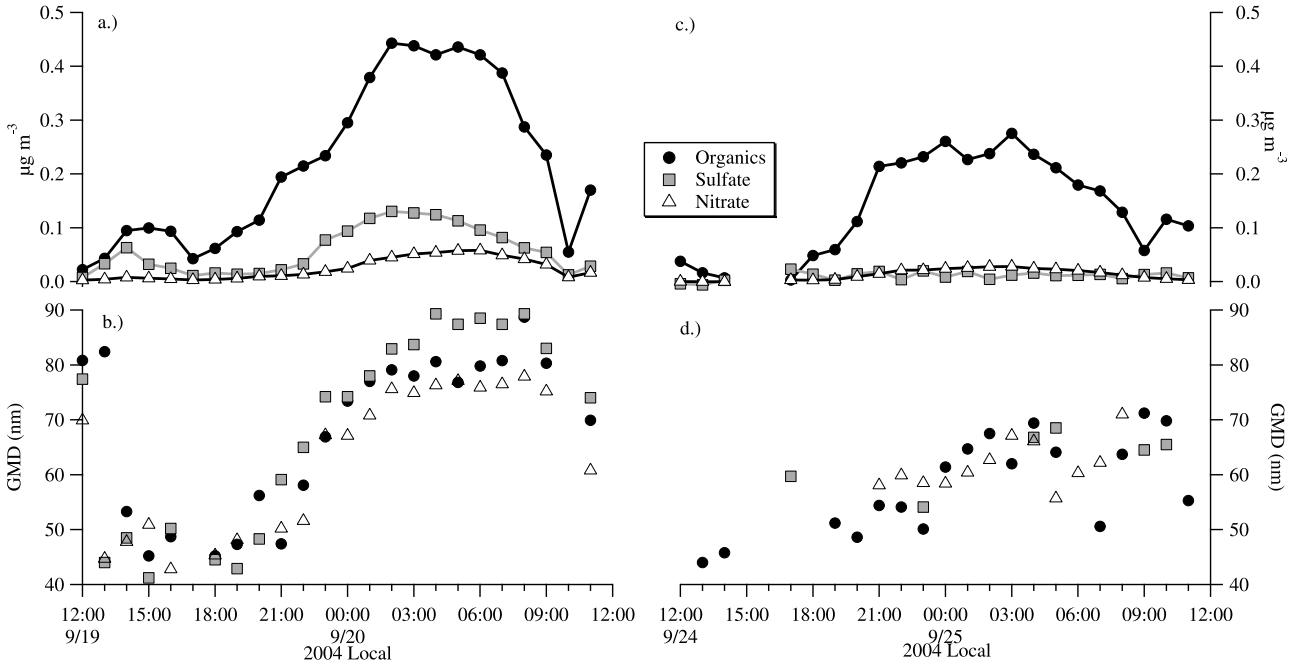

Figure 6. (a and c) Evolution of associated particle mass concentration and (b and d) GMD during E1 (Figures 6a and 6b) and E2 (Figures 6c and 6d) for organic compounds, sulfate, and nitrate. Mass concentrations include only the mass associated with the peak in dN/dlogD_{va} that occurred for sub-100 nm D_{va} particles during each event.

smaller than the average. Meteorology during E1 indicated a prevailing wind direction from the east, and backward trajectories indicated clean air mass histories from the north. Average temperatures were low (favoring partitioning of secondary material to the aerosol phase), and enhanced PAR (to drive photochemistry) was likely to influence formation of secondary aerosols.

[37] E1 exhibited relationships between the organic aerosol components and the inorganic aerosol components similar to those for the campaign average, as shown in Table 2. OOA-1 and OOA-2 exhibit enhanced correlations with toluene and isoprene and show consistent trends with isopropyl nitrate. OOA-1 and OOA-2 both show strong relationships to temperature and daytime PAR. These factors indicate the influence of temperature-driven partitioning of secondary, photochemically derived species from oxidation of both anthropogenic and biogenic parent hydrocarbons. The relationship between OOA-2 and isopropyl nitrate again points to the potential enhancement of less oxidized OA, likely of biogenic origin, by the presence of anthropogenic material.

[38] The particle size distribution during E1 was significantly different than the campaign average. The most prominent feature of the mass-based particle size distribution in Figure 4a was a peak at approximately 120 nm D_{va} that was present, but not distinct, in the campaign-average dM/dlogD_{va} shown in Figure 4c. At this E1 dM/dlogD_{va} peak, organic compounds are the dominant chemical constituent with nearly 3.5 times the mass of sulfate and 10 times that of nitrate. This distribution of mass is nearly unchanged in dM/dlogD_{va} at 60 nm D_{va}. dM/dlogD_{va} for m/z = 43 is enhanced distinctly (compared to dM/dlogD_{va} for m/z = 44) at D_{va} less than 200 nm during E1 (Figure 4a), consistent with the sub-200 nm organic aerosol during this event being less oxidized and potentially from biogenic sources. The most prominent peak in the campaign-average dM/dlogD_{va} between 300 and 400 nm D_{va} is nearly absent during E1. The number-based size distribution during E1 is characterized by an increased magnitude of the sub-100 nm D_{va} peak (by greater than a factor of two) that seems to be present beyond the Q-AMS detection limit to D_{va} smaller than 40 nm. There was negligible contribution to dN/dlogD_{va} at larger D_{va} (>200 nm) during E1. The small particles indicate the importance of more recent formation during E1.

[39] Changes in the calculated GMD were used to assess particle mass increases and GR during E1. Additionally, the chemically resolved mass concentrations associated with the peak at each GMD were calculated. Both GMD and event-associated mass concentrations are shown in Figures 6a and 6b. The calculated GMD was observed to increase linearly with time starting at 1800 on 19 September and ending at 0400 the following day. This behavior is consistent with observations of aerosol growth in many other regions of the atmosphere [*Kulmala et al.*, 2004]. The timing and calculated GR of each chemical constituent were similar, with values of 4.0, 4.9, and 3.6 nm hr^{-1} for organic compounds, sulfate, and nitrate, respectively. Correlation coefficients (R^2) for the calculation of GR were 0.95, 0.98, and 0.96 for each chemical component, respectively, indicating the linear nature of geometric growth. The similar GR values for each component suggest that the organic compounds, sulfate, and nitrate were internally mixed. An average net increase of 37 nm in D_{va} was observed during the growth event. The event-associated mass of organic compounds, sulfate, and nitrate showed increases from 1800 to

0400 local time of 0.38 μg m^{-3}, 0.11 μg m^{-3}, and 0.041 μg m^{-3}, respectively, suggesting that organic compounds contributed the majority, 71%, of the mass during the growth event. The timing of the increases in mass concentration, with varying relative amounts of organic and sulfate contribution, is also observed on other nights during the campaign (on 19 September and 27 September, for example), but smaller $N_{\text{Q-AMS}}$ made calculation of GMD impossible. Still, the timing of M_{40-60} increases on other nights suggests that particle growth is likely occurring frequently at the site and that the events presented here likely are not unique to this campaign.

3.2.2. E2

[40] During E2, total mass concentrations of inorganic aerosol constituents were also decreased relative to the campaign average (Table 1) but were larger than concentrations during E1. Concentrations of OM and the individual organic aerosol components were enhanced, though with essentially no change in their relative importance. Neutralization with respect to ammonium was more similar to the campaign average than during E1. The average spectrum of the organic aerosol during E2 (Figure 5b) was also more similar to the campaign average (including the Δ analysis) compared to E1, in that the signals from m/z 43 and m/z 44 were roughly equivalent and contributed approximately 9% each to the total organic signal. Isoprene and toluene mixing ratios were comparable to the campaign average, but that of α-pinene was decreased and that of isopropyl nitrate was enhanced. Enhanced HOA/BBOA and a more oxidized spectrum compared to E1 likely indicate an increased influence of anthropogenic organic aerosol constituents (though not compared to the campaign average). This is supported by HYSPLIT backward trajectories that traveled down the eastern seaboard of the United States for the 3 days prior to arrival at the sampling site. Unfortunately, BC, NO, O_3, and other meteorological data were unavailable during E2. Interrelationships shown in Table 2 are similar to those for E1, particularly for aerosol constituents. The relationships with VOCs are, in general, less strong, and only OOA-1 is correlated positively to isopropyl nitrate, again indicating its regional nature.

[41] The particle size distribution during E2 (Figure 4b) was more similar to the campaign-average $dM/d\log D_{va}$ (Figure 4c) than was the distribution during E1. The most prominent feature of the mass-based particle size distribution in Figure 4b was not the 120 nm D_{va} peak as in E1 but one at approximately 350 nm D_{va}, indicating the presence of larger aerosol. Still, organic compounds comprise almost twice the sulfate mass during E2. This is in contrast to the campaign-average mass distribution, which slightly favors sulfate at the peak $dM/d\log D_{va}$. This distribution is more exaggerated at 60 nm D_{va}, with organic compounds accounting for almost 20 times more mass than sulfate. The nitrate mass concentration was greater than the sulfate concentration by nearly 40%. The sub-200 nm increase in $dM/d\log D_{va}$ of m/z = 43 compared to $dM/d\log D_{va}$ of m/z = 44 is less prominent during E2 (Figure 4b) and likely indicates that biogenic oxidation products play a decreased role during E2 compared to E1. Clearly, no single factor controls growth of small particles in the suburban forest.

[42] Aerosol growth was also observed during E2, as evidenced by a linear increase in GMD (Figure 6d) and an increase in associated-particle mass concentration (Figure 6c). The timing of growth during E2 was very similar to that of E1, with increases in mass and GMD starting at approximately 1800 local time. Calculated GR for organic compounds and nitrate were 2.2 nm hr^{-1} and 1.2 nm hr^{-1} (R^2 = 0.89, R^2 = 0.82), respectively, with an average change in GMD of 21 nm D_{va}. These values were small compared to those found for E1. Few GMD values could be determined for sulfate due to very low mass concentrations during the event; therefore, no GR determination was made. The associated mass concentrations of both organic compounds and nitrate increased during the event, by 0.27 μg m^{-3} and 0.025 μg m^{-3}, respectively, suggesting that organic compounds contributed 92% of the mass increase. No significant change in associated sulfate mass concentration was observed.

4. Discussion and Conclusions

[43] Particle formation and growth events have been observed regardless of preexisting particle mass in many different locations throughout the atmosphere [*Kulmala et al.*, 2004]. Because the Duke FACE site is situated in the vicinity of a conglomerate of three moderately sized cities and experiences abundant biogenic emissions of its own, the source of new particles and condensable/condensing gases at this location is not definitive. While observation of new particle formation is not claimed in this manuscript, it is likely that the events described above are the result of the growth of newly formed particles to a size measureable by the Q-AMS. Because of nonzero wind speeds and observed GR from 1.2 to 4.9 nm hr^{-1}, the observed small particles almost certainly did not form locally at the sampling site. For example, assuming simplistically that wind speed and particle GR were constant throughout straight-line transport, new particle formation during E1 would have occurred approximately 9–10 h prior to observation by the Q-AMS, at 0700–0800 on 19 September, and approximately 80 km from the site. Particles sampled during E2, because of a smaller observed growth rate, would have a significantly larger source footprint. Therefore, the bulk composition of particles with D_{va} smaller than 40 nm that arrive at the site is representative of influence from multiple sources (local and regional) during transport and growth.

[44] During late summer, the atmosphere at the Duke FACE site appeared to be influenced to some extent by both anthropogenic and biogenic material. Regional OOA-1 and sulfate constitute significant fractions of the observed particulate matter, as does HOA/BBOA. In contrast, the OOA components do not appear as aged as those observed in other forested, rural areas [*Allan et al.*, 2006; *Cottrell et al.*, 2008], indicating a closer proximity to SOA precursor sources. This is evidenced by the increased relative importance of OOA-2 in this study.

[45] One previous study also presents Q-AMS measurements of particulate matter in the Duke Forest [*Stroud et al.*, 2007]. The previous study was conducted during July 2003. Inorganic aerosol constituents appear to have similar concentrations and variability as those presented for the current study, likely implying that anthropogenic influences between the two summer periods of different years were similar. Organic concentrations presented by *Stroud et al*. [2007] (maxima approaching 20 μg m^{-3}) are significantly larger

than those presented in the current study. Although the measurements cannot be compared directly, it is possible that this increase in OM in the study of *Stroud et al.* [2007] results from increased BVOC emission and chemistry as a result of stronger photochemistry during July relative to September. Unfortunately, an extensive spectral analysis is not presented by *Stroud et al*. [2007] so that comparisons of OM components, contributions of specific m/z, etc., are not possible. However, based on a closure study focused on prediction of cloud condensation nuclei concentrations, *Stroud et al.* [2007] inferred a mixed anthropogenic/biogenic influence on the atmosphere above the Duke FACE site, a conclusion in agreement with that of the present study.

[46] Two events were identified over the course of the campaign based on elevated number concentrations and mass concentrations of small particles. Both events exhibited linear increases in GMD and increases in mass concentration consistent with particle growth. Observed GR values between 1.2 and 4.9 nm hr^{-1} are consistent with values of between 1 and 20 nm hr^{-1} observed at other rural midlatitude sites [*Kulmala et al.*, 2004], and with an average GR of 3 nm hr^{-1} that was observed from 8 years of measurements at a boreal forest in southern Finland [*Dal Maso et al.*, 2005]. An average GR of 3.8 nm hr^{-1} was observed during summertime observations on the western slope of the Sierra Nevada Mountains of California at a site similarly located in a pine forest environment [*Lunden et al.*, 2006], a result consistent with the findings presented here. Organic compounds contributed the majority of condensed mass during both events, with only minor contribution from sulfate and nitrate. The timing of growth was similar during each event, although little consistency was observed between the two events in terms of bulk concentrations and compositions, mass-based particle size distributions, air mass history, and interrelationships among both measured and derived quantities compared to the campaign average. Thus, it appears that particle growth influenced by both local and regional sources of biogenic and anthropogenic nature occurred. This leads to the conclusion that even within forest canopies, different precursors and processes can lead to the growth of small particles. There is no apparent single variable or group of consistent variables that controls this process.

[47] **Acknowledgments.** We gratefully acknowledge the staff of Duke Forest for operation of the FACTS-1 experiment. This work was supported by the United States Environmental Protection Agency under STAR grant #RD-83145401. Additional support was provided by the UNH-NOAA AIRMAP Cooperative Institute under grant NA06OAR4600189. Qi Zhang was supported by the US Department of Energy's Atmospheric Sciences Program (Office of Science, BER), grant DE-FG02-08ER64627. These funding agencies have not reviewed this manuscript, and therefore, it does not necessarily reflect their views. No official endorsement should be inferred.

References

Allan, J. D., J. L. Jimenez, P. I. Williams, M. R. Alfarra, K. N. Bower, J. T. Jayne, H. Coe, and D. R. Worsnop (2003), Quantitative sampling using an Aerodyne aerosol mass spectrometer: 1. Techniques of data interpretation and error analysis, *J. Geophys. Res.*, *108*(D3), 4090, doi:10.1029/2002JD002358.

Allan, J. D., et al. (2004), A generalized method for the extraction of chemically resolved mass spectra from Aerodyne aerosol mass spectrometer data, *J. Aerosol Sci.*, *35*, 909–922.

Allan, J. D., et al. (2006), Size and composition measurements of background aerosol and new particle growth in a Finnish forest during QUEST 2 using an Aerodyne aerosol mass spectrometer, *Atmos. Chem. Phys.*, *6*, 315–327.

Bahreini, R., M. D. Keywood, N. L. Ng, V. Varutbangkul, S. Gao, R. C. Flagan, J. H. Seinfeld, D. R. Worsnop, and J. L. Jimenez (2005), Measurements of secondary organic aerosol from oxidation of cycloalkenes, terpenes, and m-xylene using an Aerodyne aerosol mass spectrometer, *Environ. Sci. Technol.*, *15*, 5674–5688.

Canagaratna, M., et al. (2007), Chemical and microphysical characterization of ambient aerosols with the Aerodyne aerosol mass spectrometer, *Mass Spec. Rev.*, *26*, 185–222.

Charlson, R. J., S. E. Schwartz, J. M. Hales, R. D. Cess, J. A. Coakley, J. E. Hansen, and D. J. Hofmann (1992), Climate forcing by anthropogenic aerosols, *Science*, *255*, 423–430.

Cottrell, L. D., R. J. Griffin, J. L. Jimenez, Q. Zhang, I. Ulbrich, L. D. Ziemba, P. J. Beckman, B. C. Sive, and R. W. Talbot (2008), Submicron particles at Thompson Farm during ICARTT measured using aerosol mass spectrometry, *J. Geophys. Res.*, *113*, D08212, doi:10.1029/2007JD009192.

Cwiertny, D. M., M. A. Young, and V. H. Grassian (2008), Chemistry and photochemistry of mineral dust aerosol, *Ann. Rev. Phys. Chem.*, *59*, 27–51.

Dal Maso, M., M. Kulmala, I. Riipinen, R. Wagner, T. Hussein, P. P. Aalto, and K. E. J. Lehtinen (2005), Formation and growth of fresh atmospheric aerosols: Eight years of aerosol size distribution data from SMEAR II, Hyytiälä, Finland, *Boreal Environ. Res.*, *10*, 323–336.

DeBell, L. J., M. Vozzella, R. W. Talbot, and J. E. Dibb (2004), Asian dust storm events of spring 2001 and associated pollutants observed in New England by the AIRMAP monitoring network, *J. Geophys. Res.*, *109*, D01304, doi:10.1029/2003JD003733.

deGouw, J. A., et al. (2005), Budget of organic carbon in a polluted atmosphere: Results from the New England Air Quality Study in 2002, *J. Geophys. Res.*, *110*, D16305, doi:10.1029/2004JD005623.

Draxler, R. R., and G. D. Rolph (2003), HYSPLIT (HYbrid Single-Particle Lagrangian Integrated Trajectory) Model access via NOAA ARL READY Web site, NOAA Air Resources Laboratory, Silver Spring, Md (http://www.arl.noaa.gov/ready/hysplit4.html).

Drewnick, F., J. T. Jayne, M. Canagaratna, D. R. Worsnop, and K. L. Demerjian (2004), Measurement of ambient aerosol composition during PMTACS-NY 2001 using an aerosol mass spectrometer. Part II: Chemically speciated mass distributions, *Aerosol Sci. Technol.*, *38*, 104–117.

Guenther, A., et al. (1995), A global-model of natural volatile organic-compound emissions, *J. Geophys. Res.*, *100*, 8873–8892.

Hallquist, M., et al. (2009), The formation, properties and impact of secondary organic aerosol: current emerging issues, *Atmos. Chem. Phys.*, *9*, 5155–5236.

Hari, P., M. Raivonen, T. Vesala, J. W. Munger, K. Pilegaard, and M. Kulmala (2003), Atmospheric science: Ultraviolet light and leaf emission of NO_x, *Nature*, *422*, 134.

Held, A., A. Nowak, W. Birmili, A. Wiedensohler, R. Forkel, and O. Klemm (2004), Observations of particle formation and growth in a mountainous forest region in central Europe, *J. Geophys. Res.*, *109*, D23204, doi:10.1029/2004JD005346.

Helmig, D., J. Ortega, A. Guenther, J. D. Herrick, and C. Geron (2006), Sesquiterpene emissions from loblolly pine and their potential contribution to biogenic aerosol formation in the Southeastern US, *Atmos. Environ.*, *40*, 4150–4157.

Herndon, S. C., et al. (2008), Correlation of secondary organic aerosol with odd oxygen in Mexico City, *Geophys. Res. Lett.*, *35*, L15804, doi:10.1029/2008GL034058.

Hock, B. N., et al. (2008), Rural continental aerosol properties and processes observed during the Hohenpeissenberg Aerosol Characterization Experiment (HAZE2002), *Atmos. Chem. Phys.*, *8*, 603–623.

Hoffmann, T., J. R. Odum, F. Bowman, D. Collins, D. Klockow, R. C. Flagan, and J. H. Seinfeld (1997), Formation of organic aerosols from the oxidation of biogenic hydrocarbons, *J. Atmos. Chem.*, *26*, 189–222.

Jayne, J. T., D. C. Leard, X. F. Zhang, P. Davidovits, K. A. Smith, C. E. Kolb, and D. R. Worsnop (2000), Development of an aerosol mass spectrometer for size and composition analysis of submicron particles, *Aerosol Sci. Technol.*, *33*, 49–70.

Jimenez, J. L., et al. (2003), Ambient aerosol sampling using the Aerodyne aerosol mass spectrometer, *J. Geophys. Res.*, *108*(D7), 8425, doi:10.1029/2001JD001213.

Jordan, C. E., and R. W. Talbot (2000), Direct atmospheric deposition of water-soluble nitrogen to the Gulf of Maine, *Global Biogeochem. Cycles*, *14*, 1315–1329.

Kiendler-Scharr, A., Q. Zhang, T. Hohaus, E. Kleist, A. Mensah, T. F. Mentel, C. Spindler, R. Uerlings, R. Tillmann, and J. Wildt (2009), Aerosol mass spectrometric features of biogenic SOA: Observations from a

plant chamber and in rural atmospheric environments, *Environ. Sci. Technol.*, *43*, 8166–8172.
Kroll, J. H., N. L. Ng, S. M. Murphy, R. C. Flagan, and J. H. Seinfeld (2006), Secondary organic aerosol formation from isoprene photooxidation, *Environ. Sci. Technol.*, *40*, 1869–1877.
Kulmala, M., H. Vehkamäki, T. Petäjä, M. Dal Maso, A. Lauri, V. M. Kerminen, W. Birmili, and P. H. McMurry (2004), Formation and growth rates of ultrafine atmospheric particles: A review of observations, *J. Aerosol Sci.*, *35*, 143–176.
Lanz, V. A., M. R. Alfarra, U. Baltensperger, B. Buchmann, C. Hüglin, and A. S. H. Prévôt (2007), Source apportionment of submicron organic aerosols at an urban site by factor analytical modelling of aerosol mass spectra, *Atmos. Chem. Phys.*, *7*, 1503–1522.
Liu, P., P. J. Ziemann, D. B. Kittelson, and P. H. McMurry (1995a), Generating particle beams of controlled dimensions and divergence. 1. Theory of particle motion in aerodynamic lenses and nozzle expansions, *Aerosol Sci. Technol.*, *22*, 293–313.
Liu, P., P. J. Ziemann, D. B. Kittelson, and P. H. McMurry (1995b), Generating particle beams of controlled dimensions and divergence. 2. Experimental evaluation of particle motion in aerodynamic lenses and nozzle expansions, *Aerosol Sci. Technol.*, *22*, 314–324.
Ludwig, J., F. X. Meixner, B. Vogel, and J. Forstner (2001), Soil-air exchange of nitric oxide: An overview of processes, environmental factors, and modeling studies, *Biogeochemistry*, *52*, 225–257.
Lunden, M. M., D. R. Black, M. Mckay, K. L. Revzan, A. H. Goldstein, and N. J. Brown (2006), Characteristics of fine particle growth events observed above a forested ecosystem in the Sierra Nevada Mountains of California, *Aerosol Sci. Technol.*, *40*, 373–388.
Mäkelä, J. M., I. K. Koponen, P. Aalto, and M. Kulmala (2000), One-year data of submicron size modes of tropospheric background aerosol in southern Finland, *J. Aerosol Sci.*, *31*, 595–611.
Mao, H. T., R. W. Talbot, D. Troop, R. Johnson, S. Businger, and A. M. Thompson (2006), Smart balloon observations over the North Atlantic: O_3 data analysis and modeling, *J. Geophys. Res.*, *111*, D23S56, doi:10.1029/2005JD006507.
Marquez, C., T. Castro, A. Muhlia, M. Moya, A. Martinez-Arroyo, and A. Baez (2005), Measurement of aerosol particles, gases and flux radiation in the Pico de Orizaba National Park, and its relationship to air pollution transport, *Atmos. Environ.*, *39*, 3877–3890.
McLafferty, F. W., and F. Turecek (1993), *Interpretation of Mass Spectra*, 4th ed., University Science Books, Sausalito, Calif.
Naik, V., C. Delire, C., and D. J. Wuebbles (2004), Sensitivity of global biogenic isoprenoid emissions to climate variability and atmospheric CO_2, *J. Geophys. Res.*, *109*, D06301, doi:10.1029/2003JD004236.
Odum, J. R., T. P. W. Jungkamp, R. J. Griffin, H. J. L. Forstner, R. C. Flagan, and J. H. Seinfeld (1997), Aromatics, reformulated gasoline, and atmospheric organic aerosol formation, *Environ. Sci. Technol.*, *31*, 1890–1897.
Presto, A. A., K. E. Huff-Hartz, and N. M. Donahue (2005), Secondary organic aerosol production from terpene ozonolysis. 2. Effect of NO_x concentration, *Environ. Sci. Technol.*, *39*, 7046–7054.
Schichtel, B. A., R. B. Husar, S. R. Falke, and W. E. Wilson (2001), Haze trends over the United States, 1980-1995, *Atmos. Environ.*, *35*, 5205–5210.
Schwartz, J., D. W. Dockery, and L. M. Neas (1996), Is daily mortality associated specifically with fine particles?, *JAWMA*, *46*, 927–939.
Seinfeld, J. H., and J. F. Pankow (2003), Organic atmospheric particulate material, *Ann. Rev. Phys. Chem.*, *54*, 121–140.
Sive, B. C., Y. Zhou, D. Troop, Y. L. Wang, W. C. Little, O. W. Wingenter, R. S. Russo, R. K. Varner, and R. W. Talbot (2005), Development of a cryogen-free concentration system for measurements of volatile organic compounds, *Anal. Chem.*, *77*, 6989–6998.
Smith, J. N., M. J. Dunn, T. M. VanReken, K. Iida, M. R. Stolzenburg, P. H. McMurry, and L. G. Huey (2008), Chemical composition of atmospheric nanoparticles formed from nucleation in Tecamac, Mexico: Evidence for an important role of organic species in nanoparticle growth, *Geophys. Res. Lett.*, *35*, L04808, doi:10.1029/2007GL032523.
Song, C., K. S. Na, and D. R. Cocker III (2005), Impact of the hydrocarbon to NO_x ratio on secondary organic aerosol formation, *Environ. Sci. Technol.*, *39*, 3143–3149.
Stroud, C. A., et al. (2007), Cloud activating properties of aerosol observed during CELTIC, *J. Atmos. Sci.*, *64*, 441–459.
Tsigaridis, K., and M. Kanakidou (2007), Secondary organic aerosol importance in the future atmosphere, *Atmos. Environ.*, *41*, 4682–4692.
Ulbrich, I., M. Canagaratna, Q. Zhang, D. Worsnop, and J. Jimenez (2009), Interpretation of organic components from positive matrix factorization of aerosol mass spectrometric data, *Atmos. Chem. Phys.*, *9*, 2891–2918.
White, M. L., et al. (2009), Are biogenic emissions a significant source of summertime atmospheric toluene in the rural Northeastern United States?, *Atmos. Chem. Phys.*, *9*, 81–92.
White, M. L., Y. Zhou, R. S. Russo, H. Mao, R. Talbot, R. K. Varner, and B. C. Sive (2010), Carbonyl sulfide exchange in a temperate loblolly pine forest grown under ambient and elevated CO_2, *Atmos. Chem. Phys.*, *10*, 547–561.
Zhang, Q., C. O. Stanier, M. R. Canagaratna, J. T. Jayne, D. R. Worsnop, S. N. Pandis, and J. L. Jimenez (2004), Insights into the chemistry of new particle formation and growth events in Pittsburgh based on aerosol mass spectrometry, *Environ. Sci. Technol.*, *38*, 4797–4809.
Zhang, Q., D. R. Worsnop, M. R. Canagaratna, and J. L. Jimenez (2005), Hydrocarbon-like and oxygenated organic aerosols in Pittsburgh: Insights into sources and processes of organic aerosols, *Atmos. Chem. Phys.*, *5*, 3289–3311.
Zhang, Q., et al. (2007), Ubiquity and dominance of oxygenated species in organic aerosols in anthropogenically influenced Northern Hemispheric midlatitudes, *Geophys. Res. Lett.*, *34*, L13801, doi:10.1029/2007GL029979.

P. J. Beckman, H. Mao, B. C. Sive, and R. W. Talbot, Climate Change Research Center, University of New Hampshire, Durham, NH 03824, USA.
L. D. Cottrell, Environ, Groton, MA 01450, USA.
R. J. Griffin, Department of Civil and Environmental Engineering, Rice University, Houston, TX 77005, USA. (rob.griffin@rice.edu)
R. K. Varner, Complex Systems Research Center, University of New Hampshire, Durham, NH 03824, USA.
Q. Zhang, Atmospheric Sciences Research Center, State University of New York at Albany, Albany, NY 12222, USA.
L. D. Ziemba, NASA Langley Research Center, Hampton, VA 23681-2199, USA.